HYDROLOGICAL PROCESSES
Hydrol. Process. **29**, 5337–5353 (2015)
Published online 14 July 2015 in Wiley Online Library
(wileyonlinelibrary.com) DOI: 10.1002/hyp.10553

Predicting landscape sensitivity to present and future floods in the Pacific Northwest, USA

Mohammad Safeeq,[1]* Gordon E. Grant,[1,2] Sarah L. Lewis[1] and Brian Staab[3]

[1]*College of Earth, Ocean, and Atmospheric Sciences, Oregon State University, Corvallis, OR 97331, USA*
[2]*PNW Research Station, USDA Forest Service, Corvallis, OR 97331, USA*
[3]*PNW Region, USDA Forest Service, Portland, OR 97208, USA*

Abstract:

Floods are the most frequent natural disaster, causing more loss of life and property than any other in the USA. Floods also strongly influence the structure and function of watersheds, stream channels, and aquatic ecosystems. The Pacific Northwest is particularly vulnerable to climatically driven changes in flood frequency and magnitude, because snowpacks that strongly influence flood generation are near the freezing point and thus sensitive to small changes in temperature. To improve predictions of future flooding potential and inform strategies to adapt to these changes, we mapped the sensitivity of landscapes to changes in peak flows due to climate warming across Oregon and Washington. We first developed principal component-based models for predicting peak flows across a range of recurrence intervals (2-, 10-, 25-, 50-, and 100-years) based on historical instantaneous peak flow data from 1000 gauged watersheds in Oregon and Washington. Key predictors of peak flows included drainage area and principal component scores for climate, land cover, soil, and topographic metrics. We then used these regression models to predict future peak flows by perturbing the climate variables based on future climate projections (2020s, 2040s, and 2080s) for the A1B emission scenario. For each recurrence interval, peak flow sensitivities were computed as the ratio of future to current peak flow magnitudes. Our analysis suggests that temperature-induced changes in snowpack dynamics will result in large (>30–40%) increases in peak flow magnitude in some areas, principally the Cascades, Olympics, and Blue Mountains and parts of the western edge of the Rocky Mountains. Flood generation processes in lower elevation areas are less likely to be affected, but some of these areas may be impacted by floodwaters from upstream. These results can assist land, water, and infrastructure managers in identifying watersheds and resources that are particularly vulnerable to increased peak flows and developing plans to increase their resilience. Copyright © 2015 John Wiley & Sons, Ltd.

KEY WORDS Pacific Northwest; floods; hydrologic extremes; peak flow; rain-on-snow; climate change; principal component analysis

Received 14 January 2015; Accepted 24 May 2015

INTRODUCTION

Changes in the magnitude and timing of streamflow in a warming climate pose significant risks to ecosystems, infrastructure, and the availability of water for domestic, industrial, agricultural, and recreational uses. Changes in floods are of particular concern, as they occur more frequently, affect more people, and cause more life and property damage than any other natural disaster in the USA (Kim, 2006). Yet floods do not occur uniformly across the landscape, but tend to be concentrated in particular climatic, geographic, and geological settings (O'Connor *et al.*, 2002; O'Connor and Costa, 2004a,2004b; Blöschl *et al.*, 2015). A fundamental challenge, then, is to predict how and where floods are likely to occur in the future under conditions of a rapidly changing climate.

Key to understanding the geography of past, present, and future floods is recognizing that floods result from specific hydrometeorological mechanisms that relate to both the climatic setting of watersheds and their underlying geological and geomorphic contexts (O'Connor *et al.*, 2002; Blöschl *et al.*, 2015). Both thunderstorms and hurricanes, for example, are primary weather events giving rise to the most intense precipitation events and catastrophic flooding in the Appalachian Mountains, where steep topography and shallow soils expedite delivery of water to streams (Smith *et al.*, 1996; Sturdevant-Rees *et al.*, 2001). Similarly, atmospheric rivers contribute significantly to winter floods on the west

*Correspondence to: Mohammad Safeeq, (Current affiliation) Sierra Nevada Research Institute, University of California Merced, 5200 N Lake Road, CA-95343, USA and PSW Research Station, USDA Forest Service, Fresno, CA 93710, USA.
E-mail: msafeeq@ucmerced.edu

coast of North America (Leung and Qian, 2009; Ralph *et al.*, 2006; Dettinger, 2011; Dettinger *et al.*, 2011; Neiman *et al.*, 2011) and in Western Europe (Blöschl *et al.*, 2015). Hence, predictions of future changes in flood regimes require consideration of how flood-creating mechanisms are likely to respond to different drivers of change (Merz *et al.*, 2012; Blöschl *et al.*, 2015). Based on the underlying processes, variables, and drivers of change, the processes controlling the flood regimes can be grouped into atmosphere (i.e. rainfall, snowfall, and temperature), catchments (i.e. land surface, soils, and groundwater aquifers), and river systems (characteristics of channel and flood plain) compartments (Merz *et al.*, 2012; Blöschl *et al.*, 2015). However, multiple drivers act simultaneously and interact to change flood behaviour, and the relative importance of individual drivers depends on the local situation, scale of assessment, and the boundary conditions (Blöschl *et al.*, 2015).

The largest floods in the Pacific Northwest (PNW) are generally driven by snowmelt during winter rain-on-snow events (Harr, 1981; Marks *et al.*, 1998; McCabe *et al.*, 2007). Peak flows are particularly sensitive to climate warming, because much of the snowpack in the region is considered 'warm' by climatological standards (Nolin and Daly, 2006), meaning that snow typically falls at or near the 0 °C freezing point. Thus, changes of a few degrees in temperature (Mote and Salathé, 2010; Abatzoglou *et al.*, 2014) can mean the difference between snow and rain (Nolin and Daly, 2006; McCabe *et al.*, 2007) or between snow accumulation and melt (Luce *et al.*, 2014).

The effects of climate warming on peak flows are highly uncertain and will likely vary dramatically across the landscape with the sensitivity of the precipitation regime to temperature. In higher elevation watersheds, there may be an increased risk of heavy winter rains or rain-on-snow events, both of which can cause floods. In other areas, decreased winter snowpacks resulting from a greater proportion of winter rain than snow may actually decrease the probability of rain-on-snow flooding. These potential changes pose significant challenges to land, water, and infrastructure managers. Which roads, bridges, and other infrastructure will be at a greater risk to floods? Should they be upgraded to accommodate future floods or is 'managed retreat' to safer locations a better option? If so, how should they be designed? Which streams will be subject to increased scour? Should proactive measures be implemented to reduce stream bank erosion?

Approaches to evaluating changes in floods or peak flows (we use the terms interchangeably here) generally fall into several categories. These include physically based numerical modelling and empirical statistical modelling, among others. In general, physically based numerical models predict peak flows based on detailed, coupled mathematical representations of multiple processes such as infiltration, subsurface saturated and unsaturated fluid flow, and overland and open channel flow (Freeze and Harlan, 1969; Loague and VanderKwaak, 2004). In contrast, empirical statistical models are based on observed relations between peak flows and various meteorological, hydrographic, and topographic parameters. Both approaches have strengths and weaknesses, and the ideal method for a given situation depends on many factors, including the specific questions to be addressed, the spatial and temporal scales of interest, data availability, computational capacity, and cost. Irrespective of the model, projections of meteorological and hydrographical variables from either downscaled global circulation models (GCMs) or historical trends over the last century can be incorporated to predict future changes in flood regimes (e.g. Muzik, 2002; Prudhomme *et al.*, 2003; Wilby *et al.*, 2008; Tohver *et al.*, 2014; Gyawali *et al.*, 2015).

In this paper, we analyse peak flow sensitivity to changing snowpack dynamics across Oregon and Washington. Our goal was to develop a geographically explicit model and map showing how climate warming, through its effect on where snow falls and accumulates now and in the future, is likely to change the magnitude of peak flows. The main research objectives of this study were as follows: (1) to develop a hybrid, but largely statistical, approach for peak flow prediction by integrating data from physically based numerical modelling into empirical statistical modelling; and (2) to predict the sensitivity of changes in peak flows to climate change in the PNW. Using historical instantaneous peak flow data from 1000 gauged watersheds, we built best-fit empirical regional regression models between watershed and climatic variables and peak flow for several return periods. We then evaluated future peak flow changes by perturbing the climatic variables using plausible future scenarios and calculated sensitivities as the ratio between future and present peak flows across the study domain. In this analysis, we emphasized temperature-induced changes in precipitation phase (from snow to rain) and seasonal precipitation as opposed to changes in extreme precipitation (i.e. intensities), as there is a much higher level of confidence in the former (Mote and Salathé, 2010; Abatzoglou *et al.*, 2014). Based on this and our previous work on summer low flow sensitivity (Safeeq *et al.*, 2014), managers and resource specialists can assess vulnerabilities to changing streamflows and develop adaptation plans to increase the resilience of ecosystems, infrastructure, and water supplies.

STUDY AREA

This analysis encompasses the states of Oregon and Washington located in the northwestern USA. The

elevation across this region varies from sea level to over 4300 m at Mount Rainier, with the north–south trending Cascade Range roughly dividing the western and eastern portions of the states (Figure 1). The maritime climate is highly influenced by the Pacific Ocean and varies with elevation and distance from the coast. Long-term average precipitation ranges from 150 mm in the Columbia Valley on the eastside of the Cascades to approximately 7000 mm in the Olympic Mountains (Daly *et al.*, 2008). Both Oregon and Washington have extremely wet winter and dry summer seasons, but the seasonal distribution of precipitation varies between the eastern and western halves of the region. While most of the annual precipitation occurs during fall and winter, more frequent summer thunderstorms result in a slightly higher summer precipitation in the eastern half (Mass, 2008). An altitudinal temperature gradient, varying by latitude, controls the phase of precipitation, with winter rain in lower elevations, seasonal snow at higher elevations, and transient snow at intermediate elevations (Harr, 1986; Berris and Harr, 1987; Marks *et al.*, 1998; Nolin and Daly, 2006; Jefferson, 2011). The majority of winter precipitation occurs as rain in the Coast Range and snow along the Cascades and other ranges (e.g. Okanogan highlands, Klamath, Olympics, and Blue Mountains) (Figure 1).

Previous studies have delineated broadly defined flood regions: geographic areas with similar hydrologic flood responses. In Oregon, a total of nine (seven in eastern and two in western Oregon) flood regions were delineated using a simple cluster analysis (Wiley *et al.*, 2000) on residuals from the regression between 100-year peak discharges as the response variable and drainage area as the only predictor variable (Cooper, 2005a,2005b). For Washington, a total of nine flood regions were defined on the basis of hydrologic unit boundaries (Sumioka *et al.*, 1998). We reduced the number of flood regions from this total of 18 to 8 by dissolving smaller flood regions with broadly similar topographic (e.g. Coast Range, Cascades, and Columbia plateau) and climatic (e.g. snow and rain) regimes (Figure 1). The four (region: 1, 3, 6, and 9 as defined in Sumioka *et al.*, 1998) bordering flood regions in Washington were combined with corresponding flood regions in eastern (regions 2 and 3 as defined in Cooper, 2005a) and western Oregon (regions 1 and 2 as defined in Cooper, 2005b). Prior to this, three flood regions (regions 5, 6, and 7 as defined in Sumioka *et al.*, 1998) located in Washington Columbia Plateau were merged along with two flood regions (regions 4 and 8 as defined in Sumioka *et al.*, 1998) located in Washington Okanogan highlands. Similarly, we combined region 6 (22 gauging stations, most located outside of Oregon) with adjacent regions 4 and 5 along with the 'undefined' region (Cooper, 2005a), for a total of 31 gauging stations for the new consolidated region. The aim behind reducing the number of flood regions was to enhance statistical model robustness by increasing the number of gauging stations in each individual flood region.

MATERIALS AND METHODS

Data and analysis

To build regression-based statistical models predicting flood magnitudes, we used long-term instantaneous peak

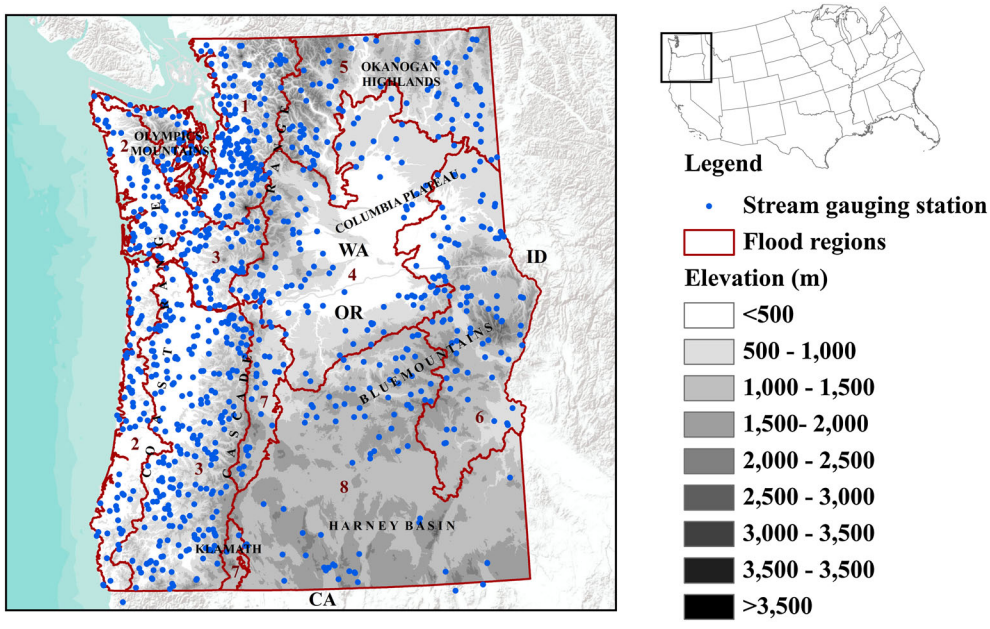

Figure 1. Study area for peak flow analysis along with stream gauging stations ($n = 1000$) and eight simplified flood regions for Oregon and Washington

flow records and extracted watershed and sub-watershed scale physiographic and climatic data relevant to flood generating processes as follows.

Peak flow data. Peak flow data, representing 2-, 10-, 25-, 50- and 100-year return periods, for 1000 U. S. Geological Survey gauging stations in Oregon and Washington were compiled from Cooper (2005a,2005b) and Sumioka *et al.* (1998), respectively (Figure 1). These peak flow values were derived by fitting a log Pearson III distribution to the historical instantaneous peak flow record (record length between 10 to 98 years), following the guidelines of U. S. Geological Survey Bulletin 17B (U.S. Water Resources Council, 1981; Advisory Committee on Water Information, 2002). Peak discharge magnitudes with a T-year return period can be calculated as

$$\log(Q_T) = \overline{Q} + KS \quad (1)$$

where $\overline{Q}$ is the mean of the logarithms of the peak discharge values, K is the frequency factor obtained from Appendix 3 of Bulletin 17B, and S is the standard deviation of the logarithms of the peak discharge values. For a detailed description of peak flow frequency analysis, refer to Cooper (2005a,2005b) and Sumioka *et al.* (1998). Watershed boundaries for all the peak flow gauges in Washington were delineated using 30-m digital elevation models (DEMs) and ArcHydro tools in ArcGIS 10.1 (ESRI, 2012). For Oregon gauges, the watershed boundary data set was acquired from the Oregon Water Resources Department (Ken Stahr, Oregon Water Resources Department, personal communication, 6 June 2014). The watershed drainage areas for these gauges range from <0.5 to 20 000 km^2 with an average value of 520 km^2. On average, the watersheds are smallest (248.6 km^2) in flood region 2 and largest (1157 km^2) in flood region 8 (Table I).

Physiographic and climate metrics

Hydraulic conductivity of soil: To characterize soil factors that control infiltration and shallow water movement, hydraulic conductivity (cm/h) data for the top 10 cm of soil (K_{soil}) were acquired from the STATSGO database (available online: http://www.cei.psu.edu). This hydraulic conductivity data set was created and is maintained by Miller and White (1998) for the conterminous USA at a 1 × 1 km spatial resolution.

Forest cover: The hydrologic response of watersheds is strongly influenced by land cover. We calculated the percentage of forest cover (FC) in each watershed after reprojecting the national land cover data set (Fry *et al.*, 2011) into a reference Universal Transverse Mercator (UTM) system and at a 30-m spatial resolution. Deciduous forest, evergreen forest, and mixed forest land cover types (Fry *et al.*, 2011) were consolidated into a single forest cover class. After consolidation, 39% of the study domain was characterized by forest, 36% by shrubs, and 9% by cultivated agriculture as single land cover types. Urban, grassland, pasture, open water and wetlands, and so on constitute the remaining 16% of the land cover. The majority of the forest cover class is located along the coast, eastern and western slopes of the Cascade Range, Klamath, Blue Mountains, Olympics Mountains, and Okanogan Highlands (Figure S1).

Topographic wetness index: We used the topographic wetness index (TWI) (Beven and Kirkby, 1979) to describe the control of local topography on hydrological processes in terms of spatial distribution of soil moisture

Table I. Average 2-, 10-, 25-, 50-, and 100-year peak flows, physiographic (DA, drainage area; TWI, topographic wetness index, K_{soil}, soil conductivity; FC, forest cover) and climate (P2, 2-year precipitation; SNR_{SF}, signal-to-noise ratio in winter snow fraction) metrics and two additional peak flow relevant watershed characteristics (T_{avg}, average winter temperature; ROS, number of winter rain-on-snow days) from the watersheds located within each flood region

		Peak flows					Physiographic and climate metrics						Additional characteristics	
Region	No. of gauges (n)	Q2	Q10	Q25	Q50	Q100	DA	P2	SNR_{SF}	TWI	FC	K_{soil}	T_{avg}	ROS
		----------(m^3/s)----------					(km^2)	(mm/day)	—	—	(%)	(cm/hr)	(°C)	(days/year)
1	198	144.2	248.6	305.0	348.6	394.3	276.4	86.2	1.9	6.9	67.2	10.2	1.6	9.2
2	123	182.6	293.9	350.9	393.6	436.7	248.6	107.4	0.7	6.5	72.9	5.4	4.7	3.0
3	300	231.9	431.7	546.1	637.3	733.3	659.6	79.2	1.2	6.7	72.1	6.1	2.6	8.0
4	101	29.9	66.4	91.7	115.3	143.2	426.2	42.7	2.1	7.1	38.5	4.9	−0.5	7.0
5	82	50.9	83.3	100.5	113.8	127.5	464.9	45.5	3.2	6.7	63.8	5.0	−2.9	8.4
6	85	28.8	61.3	82.5	100.7	121.1	647.6	34.0	1.7	6.9	38.3	3.4	−1.1	4.8
7	31	39.4	82.3	110.1	134.0	160.8	258.1	67.4	2.2	7.4	78.8	11.9	−1.3	11.5
8	80	29.7	65.0	87.1	105.5	125.4	1157.0	29.4	1.6	7.2	55.9	6.1	−1.5	5.2
All	1000	133.8	241.4	302.3	350.8	402.0	520.0	69.4	1.6	6.8	63.2	6.6	1.1	7.2

and surface saturation. The TWI was calculated using flow accumulation and slope rasters derived from the 30-m DEM as

$$\mathrm{TWI} = \frac{\ln(\mathrm{FLOWACC} * a)}{\tan(\alpha)} \quad (2)$$

where FLOWACC is the flow accumulation raster representing the upslope contributing area in the form of number of cells that flow into each cell, a is the area of each pixel in m^2, and α is the slope raster representing local gradient. For this analysis, FLOWACC raster was derived using a flow direction grid based on an eight-direction flow model. Although there has been some improvement in the flow direction algorithm (Seibert and McGlynn, 2007), evaluation of the effects of flow direction algorithm on TWI was beyond the scope of this study.

Two-year precipitation: Extreme daily precipitation (P2) representing a 2-year return period event was computed for the study domain using the generalized extreme value distribution (Chu *et al.*, 2009). We used daily 1/16th degree spatial resolution, gridded daily precipitation data sets (Table I) for the Columbia River basin and coastal drainages of Oregon and Washington from Hamlet *et al.* (2013). The Hamlet *et al.* (2013) daily precipitation data set does not cover the southern drainage basins of Oregon (i.e. Klamath and Great basins) and was supplemented with a data set covering the entire contiguous USA developed by Livneh *et al.* (2013).

Signal-to-noise ratio in winter snow fraction: The proportion of winter precipitation falling as rain or snow exerts a strong control on peak flows in this region (Tohver *et al.*, 2014). To determine the dominant precipitation type during the peak flow season, we developed a metric using daily snow-water-equivalent and precipitation data sets from Hamlet *et al.* (2013) for the Columbia River basin and coastal drainages of Oregon and Washington, and from the Bureau of Reclamation (2011) for the southern drainage basins of Oregon (Table II). We first calculated the winter snow-fraction (SF), defined as the ratio of maximum snow water equivalent ($\mathrm{SWE_{max}}$) during the winter (defined from December to March) season to the total winter precipitation (P):

$$\mathrm{SF}(\%) = \frac{\mathrm{SWE_{max}}}{P} \times 100 \quad (3)$$

Winter SF can range between 0 (when $\mathrm{SWE_{max}}$ is zero) to over 100 (when $\mathrm{SWE_{max}} > P$, e.g. higher elevations where snow starts accumulating before the winter season). We then calculated the signal-to-noise ratio (SNR) in SF to characterize the consistency in dominant precipitation regime over the length of record (1915–2006). The SNR in SF ($\mathrm{SNR_{SF}}$) was calculated as

Table II. Summary of spatially explicit data sets used in the peak flow analysis

Data set	Description	Years	Resolution	Geographic extent	Source
Peak flows	Annual maximum instantaneous peak flows at 2-, 10-, 25-, 50-, and 100-year return periods	—	Point	Oregon and Washington	Cooper (2005a,2005b); Sumioka *et al.* (1998)
Precipitation	Gridded daily precipitation	1915–2006	6 × 6 km	Columbia River basin and coastal drainages of Oregon and Washington	Hamlet *et al.*(2013)
				Southern drainage basins of Oregon	Livneh *et al.*(2013)
Snow water equivalent (SWE)	Simulated daily SWE	1915–2006	6 × 6 km	Columbia River basin and Coastal drainages of Oregon and Washington	Hamlet *et al.*(2013)
		1949–1999	12 × 12 km	Southern drainage basins of Oregon	Bureau of Reclamation (2011)
TWI	Topographic Wetness Index	—	30 × 30 m	Oregon and Washington	Developed in this study using 30-m DEM
Forest cover	Percentage of area covered by forest	2006	1 × 1 km	Oregon and Washington	Calculated in this study using national land cover data set from Fry *et al.* (2011)
Soil conductivity	Hydraulic conductivity of top 10 cm soil depth	—	1 × 1 km	Oregon and Washington	Miller and White (1998)

$$\mathrm{SNR_{SF}} = \begin{cases} 0, & mean(SF) = 0 \\ \dfrac{mean(\mathrm{SF})}{stdev(\mathrm{SF})}, & mean(SF) > 0 \end{cases} \quad (4)$$

A higher value of $\mathrm{SNR_{SF}}$ indicates that the majority of the precipitation falls as snow and varies very little from year to year. As the temperature warms, mean SF will decline and inter-annual variability in SF will likely increase, resulting in the $\mathrm{SNR_{SF}}$ distribution shifting towards zero (Figure 2).

Where necessary, all digital maps representing K_{soil}, FC, TWI, P2, and $\mathrm{SNR_{SF}}$ were re-projected into the same reference system as the DEM (Universal Transverse Mercator zone 10 and at a 30 m grid resolution). The digital maps representing physiographic and climate metrics (Figure S1) were then intersected with the delineated watersheds and 6th field (12-digit) hydrologic units, referred to as 'subwatersheds' in the National Watershed Boundary Dataset (available online at: http://nhd.usgs.gov/). Sixth-field hydrologic units were chosen because this and the next two larger scales are commonly used by government agencies and other organizations for water and other natural resource planning. Average K_{soil}, FC, TWI, P2, and $\mathrm{SNR_{SF}}$ values were computed for each of the 1000 watersheds and 4883 6th field hydrologic units using the zonal statistics within the ArcGIS Spatial Analyst.

As expected, average P2 is the highest and lowest for watersheds located in flood regions 2 and 8, respectively (Table I). The average regional precipitation at the 6th field hydrologic unit scale showed a similar pattern (Table III). Irrespective of the scale (watershed or 6th field hydrologic units), $\mathrm{SNR_{SF}}$ was the highest in flood region 5 and lowest in flood region 2. Across the region, TWI at a 30-m spatial resolution varies significantly (Figure S1). However, we found very small variability in average TWI among the different flood regions. This could be an artefact of the spatial averaging across the watersheds and hydrologic units. On average, watersheds in flood regions 4 and 6 have the lowest FC, followed by the watersheds in flood region 8 (Table I). Average percent forest cover in these watersheds is higher than the regional averages (Table III) due to the fact that most of the gauging stations are located in forested areas. Land cover in flood regions 4, 6, and 8 is predominantly characterized by shrubs and cultivated agriculture. In terms of K_{soil}, flood region 6 is the least permeable (Table I).

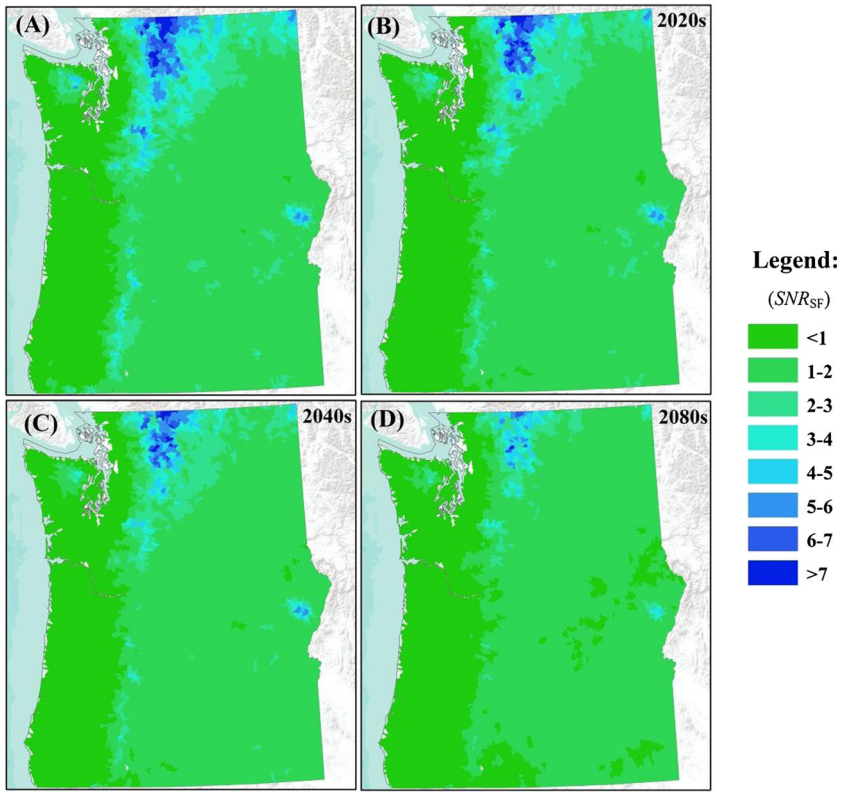

Figure 2. Comparisons of (A) 20th century $\mathrm{SNR_{SF}}$ with those projected for 21st century based on A1B emission scenarios for the (B) 2020s, (C) 2040s, and (D) 2080s, where high values indicate mostly snow with little inter-annual variation, and values approaching zero indicate little snow and high variability

Table III. Average physiographic (DA, drainage area; TWI, topographic wetness index; K_{soil}, soil conductivity; FC, forest cover) and climate (P2, 2-year precipitation; SNR_{SF}, signal-to-noise ratio in winter snow- fraction) metrics, and two additional peak flow relevant characteristics (T_{avg}, average winter temperature; ROS, number of winter rain-on-snow days) for each flood region at 6th field hydrologic unit scale

	Physiographic and climate metrics						Additional characteristics	
	DA	P2	SNR_{SF}	TWI	FC	K_{soil}	T_{avg}	ROS*
Region	(km^2)	(mm/day)	—	—	(%)	(cm/h)	(°C)	(days/year)
1	85.4	82.9	2.1	7.0	64.5	9.8	1.6	8.1
2	77.9	101.4	0.6	6.7	67.8	5.5	5.0	2.7
3	75.9	73.2	1.0	6.9	62.4	5.7	3.3	6.5
4	96.4	27.7	1.8	7.7	16.3	5.4	0.4	4.9
5	94.1	38.9	3.2	6.8	56.0	5.3	−2.9	7.3
6	79.8	27.8	1.6	7.1	27.5	3.7	−0.6	4.6
7	81.8	49.7	1.8	7.7	62.6	13.0	−0.4	9.7
8	92.6	23.9	1.5	7.8	25.2	7.7	−0.8	4.2
All	86.2	48.1	1.6	7.3	42.1	6.3	0.7	5.4

*Average ROS values were calculated after spatially interpolating the point data (Figure 3) using inverse distance weighing method

Interpretation of SNR_{SF} with respect to rain on snow. We explored the correspondence between the number of winter rain-on-snow events and SNR_{SF} in the 20th century and whether the decline in SNR_{SF} at higher elevations (Figure 2) would represent an increase in rain-on-snow events related to flooding in the 21st century. It would have been preferable to use frequency of rain-on-snow events as a metric to characterize peak flows in the region, but the resulting model would then require knowledge of the frequency of future rain-on-snow events, which is highly uncertain and not predicted by the current class of GCMs or hydrologic models.

We calculated historical frequency of rain-on-snow events using the daily precipitation and snow depth data from the 432 National Climate Data Center Coop stations and daily precipitation and snow-water-equivalent data from the 128 Natural Resources Conservation Service Snow Telemetry sites across Oregon and Washington that had 10 or more years of record between 1950 and 2013 (Figure 3). Data from the Snow Telemetry sites were used to complement the National Climate Data Center Coop stations, which are mostly located at lower elevations (McCabe *et al.*, 2007). Following McCabe *et al.* (2007), a rain-on-snow event was defined as a day when precipitation occurred and snow depth (for Coop stations) or snow water equivalent (for Snow Telemetry sites) decreased. As described by McCabe *et al.* (2007), neither all rain-on-snow events result in a lower snow depth and snow water equivalent nor are all declines in snow depth or snow water equivalent attributable to precipitation. Similarly, not all rain-on-snow events cause flooding. In order to increase the potential for flooding due to rain-on-snow events, a substantial snow depth is required, along with greater and warmer precipitation that can produce significant snowmelt; the latter is not uncommon. Hence, using this simple approach, we anticipate capturing most but not all flood related rain-on-snow events.

As expected, areas with higher rain-on-snow events are clustered along the Cascades and other mountains (e.g. Blue and Olympic) (Figure 3). On average, the

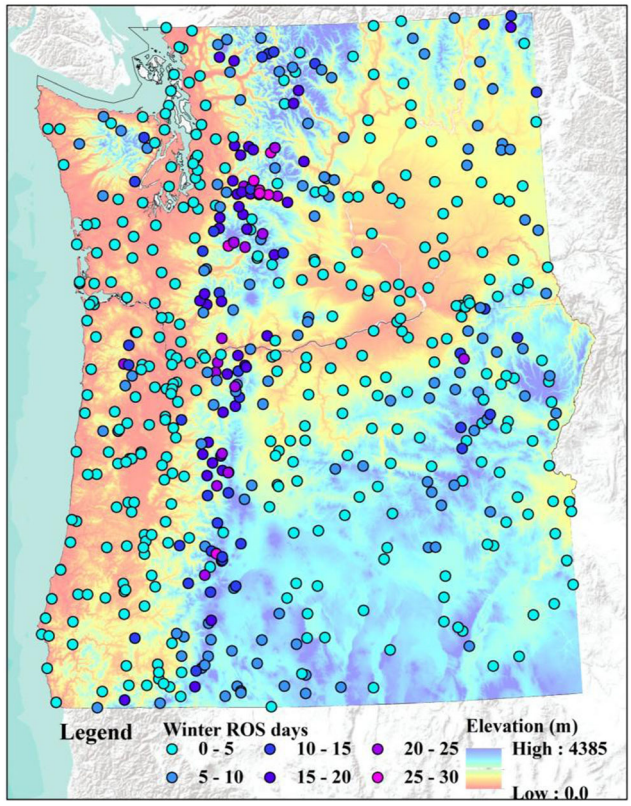

Figure 3. Annual average number of winter (defined from December to March) rain-on-snow (ROS) days across the study domain

number of rain-on-snow events is highest in the 1000–1250 m elevation range (Figure S2). McCabe *et al.* (2007) showed a positive and negative correlation between the number of rain-on-snow events and temperature (both air and sea surface) at sites over and below 1000 m elevation, respectively. As a result, under warming climate frequency of rain-on-snow events will decline at lower elevations with more precipitation falling as rain instead of snow and a fewer number of days with snow on the ground (McCabe *et al.*, 2007). At higher elevations, an increase in the number of rainy days under a warmer climate will likely increase the number of rain-on-snow events, which is consistent with the patterns developed in SNR_{SF} (Figure 2(A)). For example, the northern Cascades and other mountains (e.g. Blue and Olympic) currently have a moderate number of rain-on-snow events and have the highest SNR_{SF}. On average, higher SNR_{SF} corresponds well with the watersheds or 6th field hydrologic units located in flood regions that have cold winters and higher rain-on-snow events (Tables I and III). This demonstrates that the developed metric SNR_{SF} captures the spatial variability expressed in number of winter rain-on-snow events and average temperature across the region.

Climate change scenarios

The SNR_{SF} metric was re-calculated for future climates using the daily flux data set from Hamlet *et al.* (2013) based on statistically downscaled A1B scenarios of precipitation and temperature for the 2020s, 2040s, and 2080s using the hybrid-delta approach (Tohver *et al.*, 2014). While other (i.e. A1F1, A2, A1T, B1, and B2) scenarios are also plausible, we selected the A1B as a 'middle of the road' emission scenario, which assumes a balance between fossil fuels and other energy sources, population peaking in the middle of the 21st century, and the rapid spread of new and efficient technologies. Daily snow water equivalent and precipitation data from five 'best' GCMs (CGCM3.1(T47), CNRM-CM3, ECHAM5, ECHO, and UKMO-HadCM3) were used to calculate future SNR_{SF} for the 2020s, 2040s, and 2080s. These five GCMs were selected based on combined bias and North Pacific variability metrics (Hamlet *et al.*, 2010). SNR_{SF} values from the five GCMs were averaged and used as future scenarios (Figure 2). The future SNR_{SF} were re-sampled at 30-m spatial resolution (see Table II for native data resolution), and average indicator values were calculated for each watershed and 6th field hydrologic units using the zonal statistics within the ArcGIS Spatial Analyst. Future scenarios of SNR_{SF} for the southern drainage basins of Oregon were interpolated using a regression between the available future SNR_{SF} as the dependent variable and historic SNR_{SF}, elevation, latitude, and longitude as the independent variables (coefficient of regression, $R^2 > 0.90$).

Model development

Data normalization and transformation. For direct comparisons, five climatic and physiographic variables (P2, FC, SNR_{SF}, TWI and K_{soil}) were converted to a z-score using the following formula:

$$\delta_x = \frac{x - \overline{x}}{stdev(x)} \tag{5}$$

where δ_x is the z-score, x is the original value, and $\overline{x}$ and $stdev(x)$ are the mean and standard deviation values of the data set x, respectively.

Peak flow values (m^3/s) along with watershed drainage areas (DA, km^2) were natural-log transformed, because their distributions were highly skewed. The skewness coefficients prior to transformation were 7.1 for drainage area and ranged between 6.3 and 7.28 for peak flows. Following transformation, the skewness values ranged between 0.08 and 0.13.

Principal component analysis. Principal Component Analysis (PCA) is a statistical tool that transforms a number of potentially correlated variables into a set of uncorrelated variables that capture the variability in the underlying data. The new sets of uncorrelated variables are known as principal components. We performed PCA on the correlation matrix from the five climatic and physiographic indicators (Figure S1) using the 'stats' package in statistical software R (R Core Team, 2014). PCA on these five indicators showed strong patterns of spatial loading. The first two components (PC1 and PC2) accounted for 67% of the variation in the original five variables included in the analysis. The 3rd, 4th, and 5th principal components captured an additional 33% of the total variability (Table IV). Loadings of variables on PC1 were dominated by FC, P, and TWI (Table V). Whereas, other principal components PC2, PC3, PC4, and PC5 were dominated by SNR_{SF}, K_{soil}, P, and FC, respectively.

Table IV. Standard deviation, proportion, and cumulative variance explained by the principal components derived from climate and physiographic characteristics for all 4883 6th field hydrologic units

	Principal component number				
	1	2	3	4	5
Standard deviation	1.48	1.19	1.04	0.63	0.54
Proportion of variance explained	0.40	0.26	0.20	0.07	0.06
Cumulative variance explained	0.40	0.67	0.87	0.94	1.00

Table V. Principal component loading from principal components analysis of climate and physiographic characteristics for all 4883 6th field hydrologic units

	Principal component number				
	1	2	3	4	5
P2	0.56	−0.22	0.13	−0.73	−0.30
SNR_{SF}	0.20	0.92	−0.27	−0.20	0.07
TWI	−0.54	0.08	0.40	−0.56	0.49
FC	0.59	−0.09	0.18	0.20	0.75
K_{soil}	0.11	0.30	0.85	0.27	−0.32

Regression models of peak flows. We developed regional regression models using DA and principal component scores for climate and physiographic indicators as predictors of peak flows. The actual criteria used to determine the number of components to be retained from the PCAs are often based on the variance, which are also known as eigenvalues or the proportion of the variation in the original variables explained by the component. Kaiser's (Kaiser, 1960) criterion (eigenvalues greater than one) is commonly used for retaining principal components into the regression model. Based on Kaiser's criteria, the last two PCs, which accounted for 13% of the variability in the data set, would have been left out (Table IV). However, we chose to retain all five principal components for the regression analysis in order to account for all the variability in the independent variables (Table IV).

We overlaid the hydrologic unit maps representing the five PCs with the delineated watersheds for the streamflow gauges and computed average values for each of the 1000 watersheds. The regression model for a given peak flow (Q, m^3/s) with a specific return period T is given by:

$$\ln(Q_T) = a \times ln(\mathrm{DA}) + \sum_{i=1}^{5}(b_i \times \mathrm{PC}_i) + c \qquad (6a)$$

where DA is the watershed drainage area, PC_i is the ith principal component score, and a, b, and c are the regression coefficients. An independent variable was included in the model if it was statistically significant ($p < 0.1$). We performed the regression analysis for the entire region with all 1000 watersheds included (Figure 1) as well as for watersheds within each individual flood regions.

Peak flow sensitivity analysis

We evaluated the sensitivities of peak flows under climate change as the ratio of flood statistics between the 21st century and 20th century for the 2020s, 2040s, and 2080s. The flood ratios were calculated after re-arranging the linear regression equation (6a) as:

$$Q_T = \exp\{a \times \ln(\mathrm{DA})\} \times \exp\left\{\sum_{i=1}^{5}(b_i \times \mathrm{PC}_i) + c\right\} \qquad (6b)$$

And, peak flow sensitivity was expressed as the ratios:

$$\frac{21^{\mathrm{st}}\text{century } Q_T}{20^{\mathrm{th}}\text{century } Q_T} = \frac{\exp\left\{\sum_{i=1}^{5}\left(b_i \times PC^{i}_{21\mathrm{st\ century}}\right) + c\right\}}{\exp\left\{\sum_{i=1}^{5}\left(b_i \times PC^{i}_{20\mathrm{th\ century}}\right) + c\right\}} \qquad (7)$$

The numerator and denominator in Equation (7) are the flood magnitude under the 21st and 20th centuries, respectively. The terms $PC_{21st\ century}$ and $PC_{20th\ century}$ are the principal components derived using the five climatic and physiographic indicators (P2, FC, SNR_{SF}, TWI, and K_{soil}) for the 21st and 20th century, respectively.

RESULTS

Regression analysis

Drainage area and the five principal components of P2, SNR_{SF}, TWI, K_{soil}, and FC explain approximately 90% of the variability in peak flows (Figure 4). DA was the single most predictive variable while the five principal components derived from climate and physiographic predictors variables explain an additional 15–20% of the variance in peak flows across the range (2, 10, 25, 50, and 100 years) of recurrence intervals (Figure 4). This improvement in the regression is more pronounced for peak flows with higher recurrence intervals. The average standard error of the estimate across all the peak flows is lowered by 38% after adding the five principal components into the regression model.

The residuals from the regressions between peak flows and DA for all gauging stations show a clear divide between the eastern and western halves of the study area (Figure 5(A)). DA largely over-predicts peak flows in eastern (flood regions 4, 5, 6, 7, and 8) and under-predicts in western (flood regions 1, 2, and 3) halves. This systematic distribution of residuals is less apparent when the five principal components are included along with DA in the peak flow regression (Figure 5(B)). This pattern is consistent across all peak flows regardless of recurrence interval (Figure 6). Because there was no systematic bias in terms of residuals from the regional regression model or improvements in models (Figure S3), we do not report the regression models for individual flood regions. Rather, we used the regional regression developed using all 1000 watersheds to predict peak flows across the entire study region.

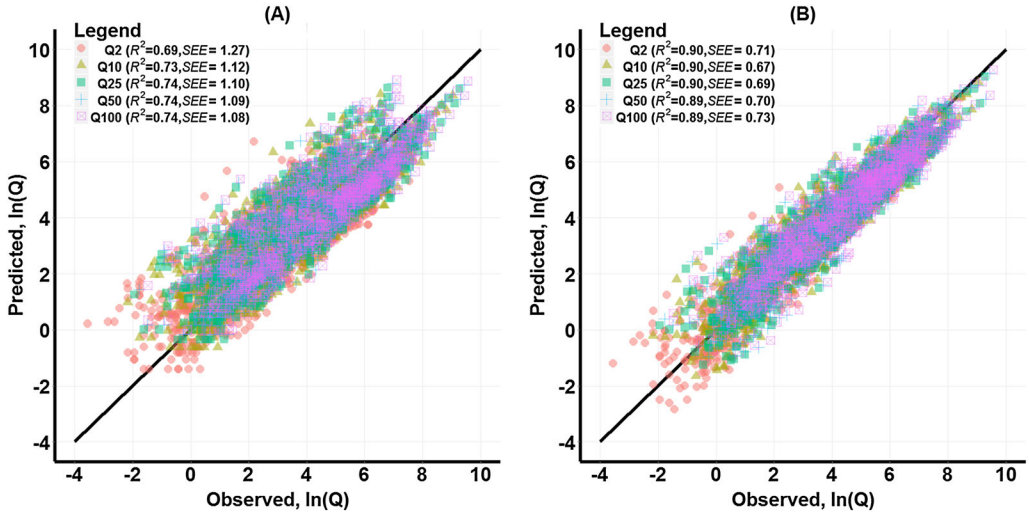

Figure 4. Comparisons of observed and predicted peak flows (Q, m^3/s)at selected recurrence intervals using (A) drainage area alone, and (B) drainage area and five principal components as predictors of peak flows

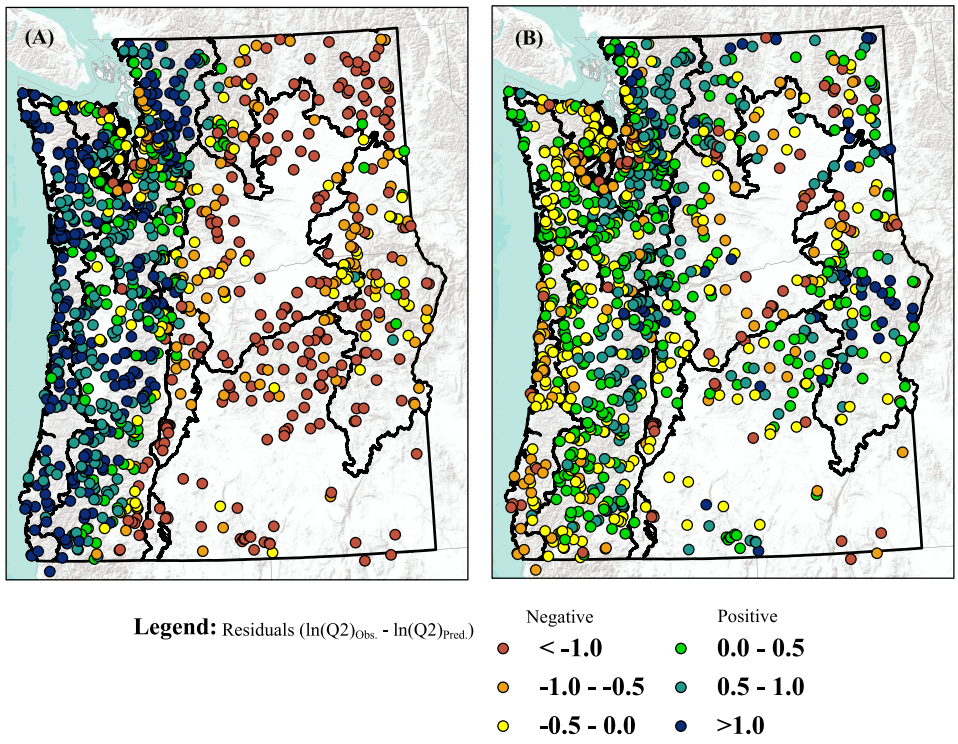

Figure 5. Spatial distribution of residuals (A) using drainage area alone as a predictor of 2-year peak flow and (B) adding five principal components along with drainage area as predictors of 2-year peak flow

The first principal component (PC1) is positively related to peak flows and DA, which is consistent with the loadings (Table V). PC2, the principal component dominated by SNR_{SF}, showed negative correlation with peak flows, indicating that an increase in SNR_{SF} corresponds to a decrease in peak flows (Table VI). Additionally, the absolute values of normalized regression coefficients for PC1 and PC2 are very comparable (Table VI). The normalized or standardized regression coefficients show the change in the dependent variable (in units of standard deviation) when an independent variable is increased by one standard deviation.

Changes in peak flows

Changes in SNR_{SF} under a future climate strongly influence flood magnitude across the study region (Figure 7). Although there is a considerable variability in the changing magnitude of flooding in different

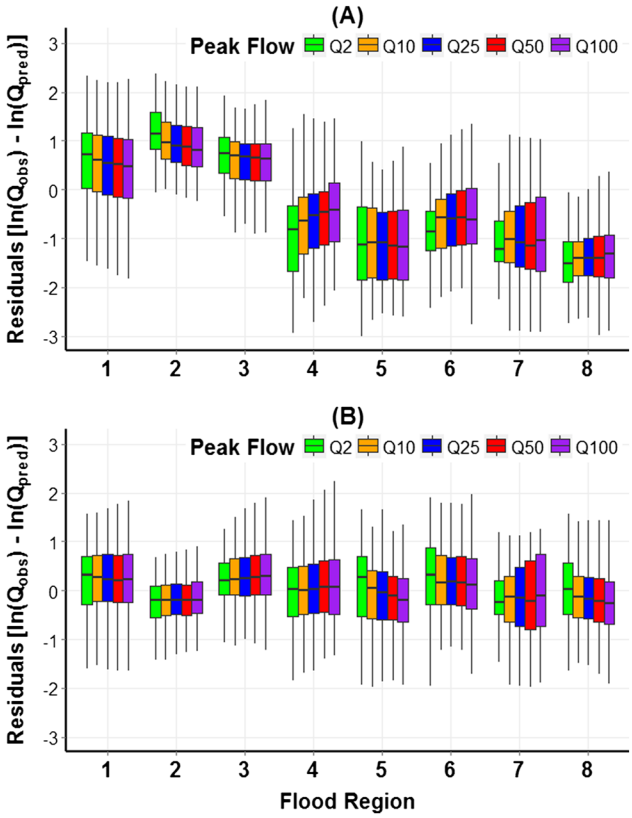

Figure 6. Average residuals across all peak flows (Q, m^3/s) and flood regions using (A) drainage area alone as a predictor of peak flows and (B) five principal components along with drainage area as predictors of peak flows. The line inside the box represents the median value, the box itself represents the interquartile range IQR (25th–75th percentile range) and the whiskers are the lowest and highest values that are within 1.5 * IQR of the 25th and 75th percentiles

watersheds, the model predicts that peak flows across the PNW will increase on average by 5%, 8%, and 15% by the 2020s, 2040s, and 2080s, respectively. Peak flows with a 2-year recurrence interval (Q2) will increase by >10% in 18%, 30%, and 53% of the study watersheds by the 2020s, 2040s, and 2080s, respectively. The percentage of watersheds with a >10% increase in peak flows with a 100-year recurrence interval (Q100) is marginally lower than Q2 (Figure 8). Nearly 12%, 22%, and 43% of the watersheds will experience a more than 10% increase in Q100 by the 2020s, 2040s, and 2080s, respectively. By the 2080s, nearly 25% of the watersheds will experience over a 20% increase in peak flows.

Watersheds with the greatest potential change in peak flows are predominantly located along the Cascades, Blue Mountains, Olympic Mountains, and parts of the western edge of the Rocky Mountains in northeast Washington (Figure 7). These watersheds have average winter temperatures below zero. The increase in peak flows diminishes exponentially with increasing winter temperatures, more so for the 2080s than the 2020s and 2040s (Figure 8). The smallest changes are expected to occur in lower elevation areas of Oregon and Washington and in the rain-dominated Oregon Coast Range, where on average, winter temperatures stay above freezing (Figure 8).

Peak flow sensitivities at the landscape scale

The results for the 6th field hydrologic units (Figure 9) show a spatial pattern of increased flood magnitudes similar to that for individual watersheds (Figure 7). The mid-to-high-elevation regions across the Cascades and Olympics show greater sensitivity to projected warming in the near term. As part of the region (especially northern Washington) shifts from snow dominated to transitional snow zone (Mantua *et al.*, 2010; Tohver *et al.*, 2014), the increase in peak flows shifts towards higher elevations (Figure 9). For example, the highest increase in peak flow by the 2020s is confined to low to mid-elevations in the northern Cascades and slowly progresses towards higher elevations by the 2040s and 2080s. By the 2080s, the Blue Mountains and parts of eastern and southern Oregon

Table VI. Summary of actual and normalized regression coefficients, adjusted coefficient of determination (Adj. R^2), and standard error of the estimate (SEE). Numbers in bold are statistically significant ($p < 0.1$)

Peak flow	Intercept	ln(DA)	PC1	PC2	PC3	PC4	PC5	Adj. R^2	SEE
				Regression coefficients					
Q2	**−1.408**	**0.876**	**0.561**	**−0.418**	**0.082**	**−0.568**	**−0.620**	0.90	0.71
Q10	**−0.519**	**0.869**	**0.415**	**−0.360**	0.001	**−0.485**	**−0.770**	0.90	0.67
Q25	**−0.199**	**0.865**	**0.369**	**−0.338**	−0.026	**−0.453**	**−0.821**	0.90	0.69
Q50	0.006	**0.864**	**0.338**	**−0.324**	−0.043	**−0.434**	**−0.853**	0.89	0.70
Q100	**0.191**	**0.862**	**0.313**	**−0.312**	**−0.059**	**−0.416**	**−0.882**	0.88	0.73
				Normalized regression coefficients					
Q2	—	0.835	0.285	−0.211	0.025	−0.135	−0.120	—	—
Q10	—	0.868	0.221	−0.191	0.000	−0.121	−0.156	—	—
Q25	—	0.874	0.199	−0.182	−0.008	−0.114	−0.169	—	—
Q50	—	0.877	0.183	−0.175	−0.014	−0.110	−0.176	—	—
Q100	—	0.879	0.170	−0.169	−0.019	−0.106	−0.183	—	—

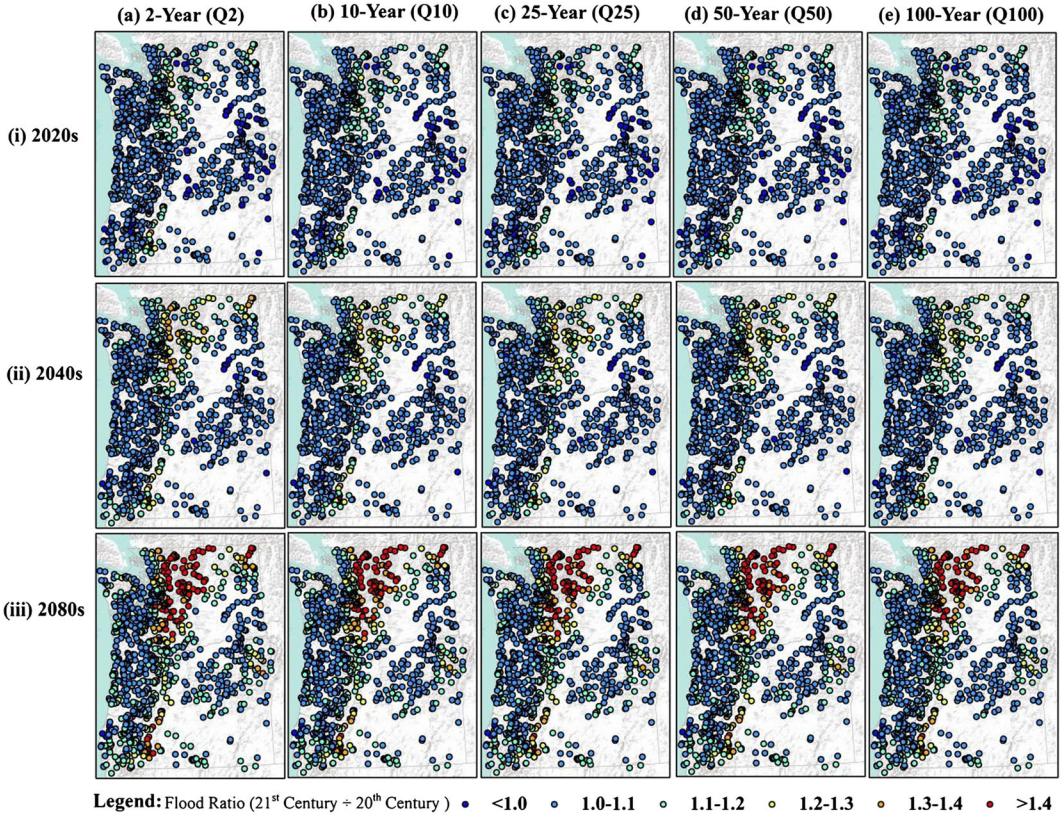

Figure 7. Changes in peak flows (A–E) between historic and future climate under A1B emission scenario for the (i) 2020s, (ii) 2040s, and (iii) 2080s at 1000 gauging stations. Changes in peak flows are calculated as the ratio (higher ratios indicate more intense flooding events projected for the future) of flood magnitude between the 21st century and 20th century

will become more sensitive to climate warming. As the temperature continues to warm, this shift in peak flow sensitivity becomes quite prominent. By the 2020s, only 8% of the region shows a 10% or higher peak flow increase, but this doubles by the end of the 2080s. Similarly, increases in peak flow of 20% or more are expected to be very limited (<2% of the region) by the end of the 2020s, but become more widespread (16% of the region) by the end of the 2080s. This pattern is quite consistent across the 2-, 10-, 25-, 50-, 100-year peak flows (Figure S4).

DISCUSSION

Hydrologic effects of climate change across the Pacific Northwest and much of the western USA has long been acknowledged. However, efforts have been mostly directed towards understanding changes in snowpack (Mote *et al.*, 2005; Hamlet *et al.*, 2005; Nolin and Daly, 2006; Luce *et al.*, 2014) and the timing and magnitude of streamflow (Ragonda *et al.*, 2005; Stewart *et al.*, 2005; Barnett *et al.*, 2005, 2008; Luce and Holden, 2009; Das *et al.*, 2011; Safeeq *et al.*, 2013). Despite a well-founded interpretation of diminishing mountain snowpack and its effect on hydrologic regimes of the region's rivers and streams, regional-scale studies of changes in peak flows are limited (e.g. Hamlet and Lettenmaier, 2007; Tohver *et al.*, 2014). This is in part due to the complexity of flood-generation mechanisms and dominant controls (both climatic and non-climatic) that vary systematically in both space and time. Regional-scale modelling of peak flows under climate change using physically based hydrologic models, which has been the most common approach to date, poses greater challenges than modelling of smoothed metrics like mean monthly or seasonal flows. To overcome some of these challenges, especially in data-limited regions and ungauged basins, regional regression models are developed as an alternative for climate change impact assessments (Fennessey, 1994, 2010; Gyawali *et al.*, 2015). However, regional regression models have their own limitations (Gyawali *et al.*, 2015) and may often require hydro-climatological data that are not available (e.g. spatially distributed snowpack). In this study, we have bridged the gap and successfully illustrated how modelled hydro-climatological data such as snow accumulation and melt can be utilized in developing regional regression models for large-scale assessments of climate change impacts. Our results demonstrate that broad scale snow-water-equivalent products developed for monthly and seasonal-scale water resource evaluation can be trans-

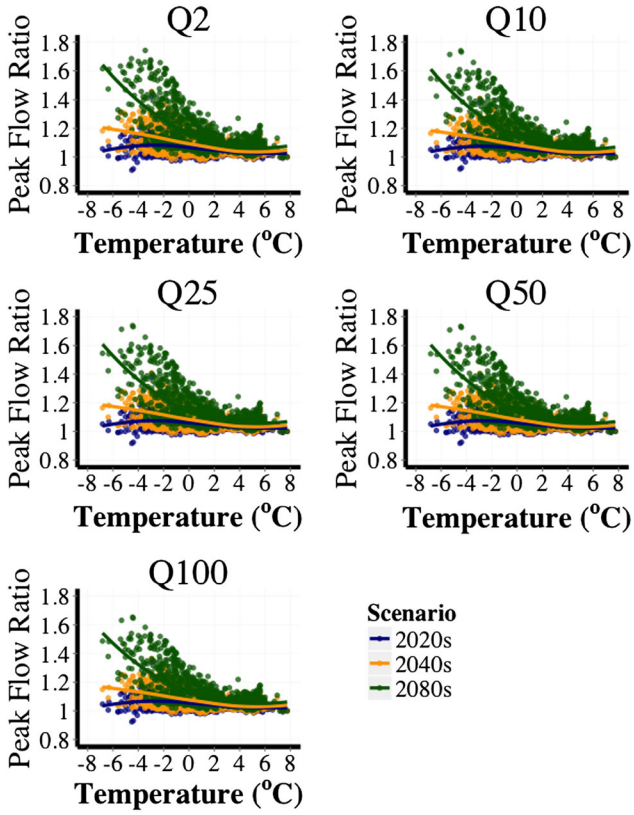

Figure 8. Peak flow ratio (21st century Q ÷ 20th century Q) as a function of watershed average winter temperature for the 2020s, 2040s, and 2080s. The solid line shows locally weighted smoothing using LOESS method

formed based on process linkages and utilized in regional regression models for peak flow prediction.

The magnitudes of peak flow change presented here are similar to those of Tohver *et al.* (2014) for the Olympic Mountains and central Cascade Mountains. Our predictions are, however, slightly higher for the Rockies, slightly lower for the Northern Cascades, and substantially lower for the Blue Mountains than found by Tohver *et al.* (2014). There are several reasons for these differences. First, while both studies used some of the same driving data (e.g. snow water equivalent), the methods for predicting changes in peak flows were very different. Tohver *et al.* (2014), for example, used the physically based Variable Infiltration Capacity model (Liang *et al.*, 1994), while we employed an empirical regression-based approach. Moreover, our results only consider peak flow changes associated with snowpack dynamics due to changes in precipitation phase (from snow to rain) and seasonal precipitation, whereas Tohver *et al.* (2014) also considered potential changes stemming from shifts in extreme precipitation. We did not consider changes in precipitation (i.e. 2-year precipitation) due to large uncertainties in its direction and magnitude (Abatzoglou *et al.*, 2014; Mote and Salathé, 2010).

Other studies on the effects of climate change on peak flows have been conducted in areas outside the PNW. Muzik (2002), for example, reported a 40% and 80% increase in the 2-year and 100-year flows, respectively, in a Rocky Mountain subalpine watershed as a result of 25% increase in the mean and standard deviation of 6- and 48-hour precipitation alone. For the Rhine River in Europe, Kwadijk and Middelkoop (1994) reported a 30% increase in 2-year peak flow in response to a 20% increase in annual precipitation. Reynard *et al.* (2001) showed a 3–47% increase in peak daily flows of difference recurrence intervals in two UK catchments. These varying magnitudes of peak flow change, some of which are attributed to the way climate change scenarios are implemented, only provide a context and highlight the spatial variability in precipitation-related increases in peak flows.

Besides altered precipitation and temperature regimes, changes in forest cover can affect peak flows (Table V). It is unclear on how land use and forest management practices in the Pacific Northwest will change over time. However, with diminishing snowpack (Mote *et al.*, 2005) and increasing fire activity (Westerling *et al.*, 2006; Dennison *et al.*, 2014), a 78% increase in forest area burned is expected for the Pacific Northwest by the middle of the 21st century (Spracklen *et al.*, 2009). Similarly, drought-caused and insect-caused tree mortalities pose additional threats to the forested landscapes (Grant *et al.*, 2013). All of these factors could potentially amplify the changes in peak flows considered in our analysis. However, the impact of forest cover is not uniform across all peak flows. The rate of peak flow increase (in the case of deforestation) or decrease (in the case of afforestation) declines exponentially with increasing peak flow magnitude (Salazar *et al.*, 2012; Blöschl *et al.*, 2015). Additionally, unlike climate variability, the impact of land use on flood magnitude diminishes with increasing catchment scale (Blöschl *et al.*, 2007; Blöschl *et al.*, 2015), and hence, the scale of assessment becomes important.

MANAGEMENT IMPLICATIONS

Our results can assist managers in implementing a variety of climate change policies-related infrastructure. The U.S. Federal Government, for example, recently established a Federal Flood Risk Management Standard that seeks to reduce the risk and cost of future flood disasters by requiring all federal investments in and affecting floodplains to meet higher flood risk standards (Exec. Order No. 11988, Amended, 2015). Specifically, the standard requires agencies to identify flood elevation and hazard areas and manage risks through proper siting, design, and construction by (1) using data and methods

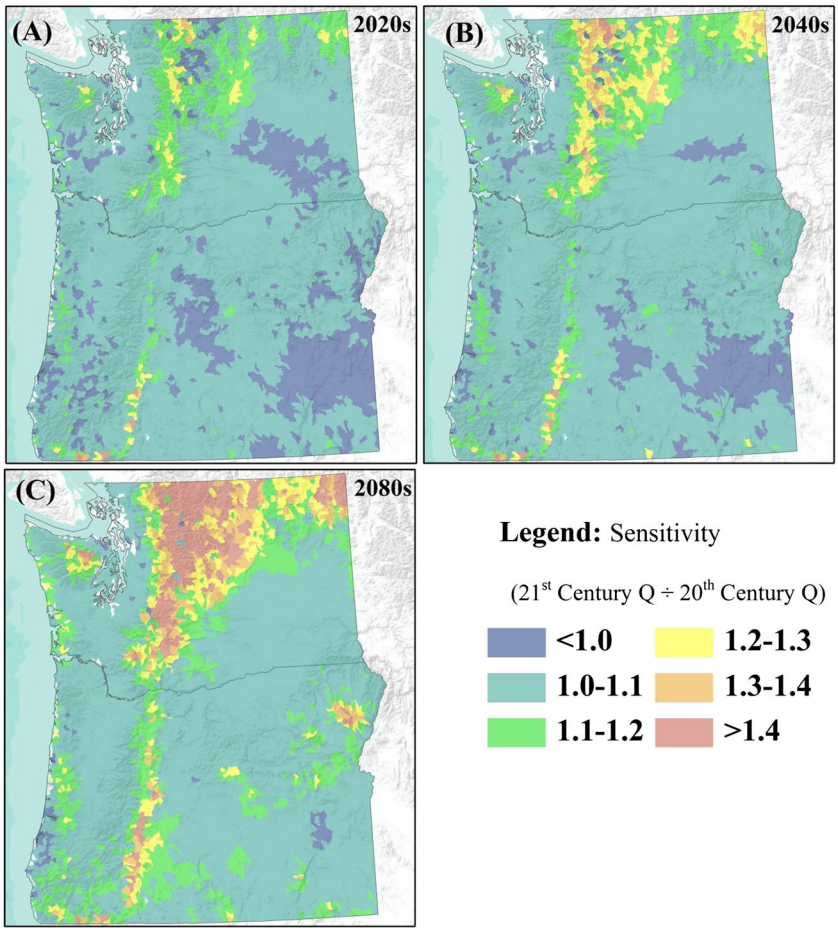

Figure 9. Six field hydrologic unit scale average peak flow sensitivities across all flood magnitudes (Q2, Q10, Q25, Q50, and Q100) under A1B emission scenario for the (A) 2020s, (B) 2040s, and (C) 2080s, where red is more sensitive and blue is less sensitive. Sensitivities for individual flood statistics for 2-, 10-, 25-, 50-, and 100-year recurrence intervals are shown in appendix Figure S4

informed by best-available, actionable climate science; (2) building 2 ft above the 100-year flood elevation for standard projects, and 3 ft above for critical buildings like hospitals and evacuation centres; or (3) building to the 500-year flood elevation. Our models and results could be used as one component of option 1 for meeting the new standard, which is perhaps the most effective and economical one. These products could inform management of infrastructure outside of floodplains as well. For example, key water supplies in the PNW, such as those supporting the cities of Portland and Salem, Oregon, are vulnerable to large floods. These events can force managers to shut down municipal water treatment systems for days or weeks due to excessive turbidity caused by the mobilization and transport of microscopic clay particles from upstream watersheds and stream channels (LaHusen, 1994; Government Accountability Office, 1998). Our analysis could be used to identify areas that may be more susceptible to such events in the future, and this enables implementation of adaptation actions, such as the development or augmentation of back-up water supplies.

Increased flood frequency and magnitude pose significant threats to other resources as well, such as aquatic ecosystems. In the PNW, recovery of several species of Pacific salmon listed under the Endangered Species Act is a significant issue with many environmental, social, and economic dimensions. Each year, for example, more than $300 million is spent in the Columbia River basin alone to restore habitats degraded by past and ongoing land uses, water management, and other activities (Rieman *et al.*, 2015). It is increasingly recognized that climate change will interact with these existing impacts, often exacerbating their effects. Battin *et al.* (2007), for example, concluded that the largest single driver of future climate-induced population declines in the Snohomish River basin in western Washington will likely be the impact of increased peak flows on egg survival. At the broad scale, our results could be used to identify watersheds and populations most at risk of these types of effects. At finer scales, they could be combined with geomorphic, ecological, and land use data (e.g. artificially confined channels, substrate composition, and key spawning areas) to identify stream reaches most

susceptible to increased redd scour and reveal opportunities for restoration (e.g. setback levees).

LIMITATIONS

As described earlier, our analysis only considers the effects of temperature-induced changes in precipitation phase (i.e. snow *vs* rain) and seasonal precipitation. It does not consider the effects of potential changes in timing, magnitude, and frequency of extreme precipitation. Thus, the results may under-estimate or over-estimate the magnitude of increased flood risk. Similarly, we did not consider the potential for climate change to alter the frequency, magnitude, timing, or location of atmospheric rivers, which play an important role in generating big storms and floods in this region (Leung and Qian, 2009; Ralph *et al.*, 2006; Dettinger, 2011; Dettinger *et al.*, 2011; Neiman *et al.*, 2011) as well as in other parts of the world (Blöschl *et al.*, 2015). Moreover, the regression equations developed in this study are based on unregulated streamflows and thus do not account for reservoir operations, diversion, or any other form of water withdrawal from the streams. Hence, depending on the level of regulation, the projected increases in peak flows presented here may not represent realized conditions.

A more subtle bias in this analysis is that our models are constrained by the past and present distributions of stream gauges used to develop the models. There are areas of the study domain that are 'gauge-poor' in that the number of gauges and years of record measured are sparse; hence, the models under-represent peak flow processes in these areas. These areas include the higher elevations of the Cascades, many of which are underlain by young, highly permeable, volcanic rocks that tend to store water, dampen translation of recharge-induced pressure waves, and, hence, tend to have more muted hydrograph responses and peak flows (Grant, 1997; Jefferson *et al.*, 2008, 2010). Having a larger number of such basins represented in our overall sample might have changed the model structure somewhat. Other hydrologic modelling suggests, however, that the High Cascades will experience peak flow increases in the future on the same order as suggested by this study (Tague and Grant, 2009). Similar caveats apply to other data-poor areas, such as eastern Oregon and Washington.

SUMMARY AND CONCLUSIONS

We developed regression models to predict peak streamflows with 2-, 10-, 25-, 50-, and 100-year recurrence intervals based on climatic and physiographic metrics. The models were used to predict peak flows under current conditions and for the 2020s, 2040s, and 2080s under the A1B emission scenario. To address multicollinearity, we used principal component analysis to convert all independent variables into components or scores that are orthogonal to each other. Our results provide landscape-scale maps that identify watersheds that are predicted to be most and least sensitive to peak flow changes under warming-induced changes in precipitation phase and snowpack dynamics. These maps highlight the importance of how changing the dominant phase of precipitation from snow to rain is likely to affect geomorphically and ecologically effective flows in this region. Moreover, these results indicate that changes are progressive across elevation ranges and landscapes as warming proceeds throughout this century. Together with information regarding the location and sensitivity of key infrastructure, habitats, or other resources of interest, these maps and analyses can be used to assess vulnerabilities and develop plans to adapt to potentially challenging hydrologic conditions.

ACKNOWLEDGEMENTS

The authors gratefully acknowledge Rachel LovellFord, Hydrologist at the Oregon Water Resources Department, for providing the digital watershed boundary data and Ivan Arismendi, Assistant Professor Senior Researcher at the Oregon State University, for providing insights on principal component analysis. They acknowledge funding support from the Oregon Watershed Enhancement Board, the Bureau of Land Management (Oregon) and the USDA Forest Service Region 6 and Pacific Northwest Research Station.

REFERENCES

Abatzoglou JT, Rupp DE, Mote PW. 2014. Seasonal climate variability and change in the Pacific Northwest of the United States. *Journal of Climate* **27**: 2125–2142. DOI:10.1175/JCLI-D-13-00218.1.

Advisory Committee on Water Information. 2002. Bulletin 17-B Flood Frequency Guidelines, Frequently Asked Questions: U.S. Geological Survey, Online: http://water.usgs.gov/osw/bulletin17b/bulletin_17B.html (Last accessed on 22 May 2015).

Barnett TP, Adam JC, Lettenmaier DP. 2005. Potential impacts of a warming climate on water availability in snow-dominated regions. *Nature* **438**(7066): 303–309.

Barnett TP, Pierce DW, Hidalgo HG, Bonfils C, Santer BD, Das T, Bala G, Wood AW, Nozawa T, Mirin AA, Cayan DR, Dettinger MD. 2008. Human-induced changes in the hydrology of the western United States. *Science* **319**(5866): 1080–1083.

Battin J, Wiley MW, Ruckelshaus MH, Palmer RN, Korb E, Bartz KK, Imaki H. 2007. Projected impacts of climate change on salmon habitat restoration. *Proceedings of the National Academy of Sciences* **104**(16): 6720–6725.

Berris SN, Harr RD. 1987. Comparative snow accumulation and melt during rainfall in forested and clear-cut plots in the Western Cascades of Oregon. *Water Resources Research* **23**(1): 135–142.

Beven K, Kirkby M. 1979. A physically based, variable contributing area model of basin hydrology. *Hydrological Sciences Journal* **24**: 43–69.

Blöschl G, Ardoin-Bardin S, Bonell M, Dorninger M, Goodrich D, Gutknecht D, Matamoros D, Merz B, Shand P, Szolgay J. 2007. At

what scales do climate variability and land cover change impact on flooding and low flows? *Hydrological Processes* **21**(9): 1241–1247.

Blöschl G, Gaál L, Hall J, Kiss A, Komma J, Nester T, Parajka J, Perdigão RAP, Plavcová L, Rogger M, Salinas JL, Viglione A. 2015. Increasing river floods: fiction or reality? *Wiley Interdisciplinary Reviews: Water* . DOI:10.1002/wat2.1079.

Bureau of Reclamation. 2011. SECURE Water Act Section 9503(c) – reclamation climate change and water, report to congress, 2011.

Chu PS, Zhao X, Ruan Y, Grubbs M. 2009. Extreme rainfall events in the Hawaiian Islands. *Journal of Applied Meteorology and Climatology* **48**: 502–516.

Cooper RM. 2005a. Estimation of peak discharges for rural, unregulated streams in eastern Oregon, Oregon Water Resources Department Open File Report SW 06-001.150 p.

Cooper RM. 2005b. Estimation of peak discharges for rural, unregulated streams in western Oregon. Scientific Investigations Report 2005-5116. Reston, VA: U.S. Geological Survey, 134.

Dettinger MD. 2011. Climate change, atmospheric rivers, and floods in California – a multimodel analysis of storm frequency and magnitude changes. *Journal of the American Water Resources Association (JAWRA)* **47**(3): 514–523. DOI:10.1111/j.1752-688.2011.00546.x.

Dettinger MD, Ralph FM, Das T, Neiman PJ, Cayan DR. 2011. Atmospheric rivers, floods and the water resources of California. *Water* **3**(2): 445–478.

Das T, Pierce DW, Cayan DR, Vano JA, Lettenmaier DP. 2011. The importance of warm season warming to western US streamflow changes. *Geophysical Research Letters* **38**: L23403. DOI:10.1029/2011GL049660.

Daly C, Halbleib M, Smith JI, Gibson WP, Doggett MK, Taylor GH, Curtis J, Pasteris PP. 2008. Physiographically sensitive mapping of climatological temperature and precipitation across the conterminous United States. *International Journal of Climatology* **28**: 2031–2064.

Dennison PE, Brewer SC, Arnold JD, Moritz MA. 2014. Large wildfire trends in the western United States, 1984–2011. *Geophysical Research Letters* **41**(8): 2928–2933.

ESRI. 2012. *ArcGIS Desktop: Release 10.1*. Environmental Systems Research Institute: Redlands, CA.

Exec. Order No. 11988, Amended. 2015. Establishing a Federal Flood Risk Management Standard and a process for further soliciting and considering stakeholder input.

Fry JA, Xian G, Jin S, Dewitz JA, Homer CG, Limin Y, Barnes CA, Herold DN, Wickham JD. 2011. Completion of the 2006 national land cover database for the conterminous United States. *Photogrammetric Engineering and Remote Sensing* **77**: 858–864.

Fennessey NM. 1994. A hydro-climatological model of daily streamflow in the Northeast United States. PhD Thesis, Tufts University, August, 1994.

Fennessey NM. 2010. Potential climate change impacts to streamflow in the Northeast U.S., ASCE EWRI World Environmental & Water Resources Congress, Providence, RI. May 16–20.

Freeze RA, Harlan RL. 1969. Blueprint for a physically-based digitally simulated, hydrologic response model. *Journal of Hydrology* **9**: 237–258.

Government Accountability Office. 1998. Oregon Watersheds: many activities contribute to increased turbidity during large storms. GAO/RCED-98-220.

Grant GE. 1997. A geomorphic basis for interpreting the hydrologic behavior of large river basins. In *River Quality: Dynamics and Restoration*, Laenan A (ed.). CRC Lewis Publishers: 105–116.

Grant GE, Tague CL, Allen CD. 2013. Watering the forest for the trees: an emerging priority for managing water in forest landscapes. *Frontiers in Ecology and the Environment* **11**(6): 314–321.

Gyawali R, Griffis VW, Watkins DW, Fennessey NM. 2015. Regional regression models for hydro-climate change impact assessment. *Hydrological Processes* **29**(8): 1972–1985. DOI:10.1002/hyp.10312.

Hamlet AF, Mote PW, Clark MP, Lettenmaier DP. 2005. Effects of temperature and precipitation variability on snowpack trends in the Western United States. *Journal of Climate* **18**(21): 4545–4561.

Hamlet AF, Lettenmaier DP. 2007. Effects of 20th century warming and climate variability on flood risk in the western U.S. *Water Resources Research* **43**: W06427. DOI:10.1029/2006WR005099.

Hamlet AF, Salathé EP, Carrasco P. 2010. Statistical downscaling techniques for global climate model simulations of temperature and precipitation with application to water resources planning studies. The Columbia Basin Climate Change Scenarios Project (CBCCSP) report (available online: http://warm.atmos.washington.edu/2860/report/) (Last accessed on 22 May 2015).

Hamlet AF, Elsner MM, Mauger GS, Lee SY, Tohver I, Norheim RA. 2013. An overview of the Columbia basin climate change scenarios project: approach, methods, and summary of key results. *Atmosphere-Ocean* **51**: 392–415.

Harr RD. 1986. Effects of clearcutting on rain-on-snow runoff in western Oregon: a new look at old studies. *Water Resources Research* **22**(7): 1095–1100.

Harr RD. 1981. Some characteristics and consequences of snowmelt during rainfall in western Oregon. *Journal of Hydrology* **53**: 277–304.

Jefferson A, Nolin A, Lewis SL, Tague CL. 2008. Hydrogeologic controls on streamflow sensitivity to climate variation. *Hydrological Processes* **22**: 4371–4385.

Jefferson A, Grant GE, Lewis SL, Lancaster ST. 2010. Coevolution of hydrology and topography on a basalt landscape in the Oregon Cascade Range, USA. *Earth Surface Processes and Landforms* **35**(7): 803–816.

Jefferson AJ. 2011. Seasonal versus transient snow and the elevation dependence of climate sensitivity in maritime mountainous regions. *Geophysical Research Letters* **38**: L16402. DOI:10.1029/2011GL048346.

Kaiser HF. 1960. The application of electronic computers to factor analysis. *Educational and Psychological Measurement* **20**: 141–151.

Kim SH. 2006. Flood. In *Disaster Medicine*, 3rd edn, Ciottone G (ed.). Mosby Elsevirr: Philadelphia, PA.

Kwadijk J, Middelkoop H. 1994. Estimation of impact of climate change on the peak discharge probability of the river Rhine. *Climatic Change* **27**(2): 199–224.

LaHusen RG. 1994. Variations in turbidity in streams of the Bull Run Watershed, Oregon 1989-90. Water-Resources Investigations Report 93–4045, Vancouver, Wash.: Denver, CO: U.S. Dept. of the Interior, U.S. Geological Survey; Earth Science Information Center, Open-File Reports Section [distributor].

Liang X, Lettenmaier DP, Wood EF, Burges SJ. 1994. A simple hydrologically based model of land surface water and energy fluxes for GSMs. *Journal of Geophysical Research* **99**(D7): 14,415–14,428.

Leung LR, Qian Y. 2009. Atmospheric rivers induced heavy precipitation and flooding in the western US simulated by the WRF regional climate model. *Geophysical Research Letters* **36**: L03820. DOI:10.1029/2008GL036445.

Livneh B, Rosenberg EA, Lin C, Nijssen B, Mishra V, Andreadis KM, Maurer EP, Lettenmaier DP. 2013. A long-term hydrologically based dataset of land surface fluxes and states for the conterminous United States: update and extensions. *Journal of Climate* **26**: 9384–9392.

Loague K, VanderKwaak JE. 2004. Physics-based hydrologic response simulation: platinum bridge, 1958 Edsel, or useful tool. *Hydrological Processes* **18**: 2949–2956.

Luce CH, Holden ZA. 2009. Declining annual streamflow distributions in the Pacific Northwest United States, 1948–2006. *Geophysical Research Letters* **36**(16): . DOI:10.1029/2009GL039407.

Luce CH, Lopez-Burgos V, Holden Z. 2014. Sensitivity of snowpack storage to precipitation and temperature using spatial and temporal analog models. *Water Resources Research* **50**. DOI:10.1002/2013WR014844.

Mantua N, Tohver I, Hamlet A. 2010. Climate change impacts on streamflow extremes and summertime stream temperature and their possible consequences for freshwater salmon habitat in Washington State. *Climatic Change* **102**: 187–223.

Marks D, Kimball J, Tingey D, Link T. 1998. The sensitivity of snowmelt processes to climate conditions and forest cover during rain-on-snow: a case study of the 1996 Pacific Northwest flood. *Hydrological Processes* **12**: 1569–1587.

Mass C. 2008. *The Weather of the Pacific Northwest*. University of Washington Press: Seattle, Washington, USA.

McCabe GJ, Hay LE, Clark MP. 2007. Rain-on-snow events in the western United States. *Bulletin of the American Meteorological Society* **88**: 319–328.

Merz B, Vorogushyn S, Uhlemann S, Delgado J, Hundecha Y. 2012. HESS opinions—more efforts and scientific rigour are needed to attribute trends in flood time series. *Hydrology and Earth System Sciences* **16**: 1379–1387.

Miller DA, White RA. 1998. A conterminous United States multilayer soil characteristics dataset for regional climate and hydrology modeling. *Earth Interactions* **2**: 1–26.

Mote PW, Hamlet AF, Clark MP, Lettenmaier DP. 2005. Declining mountain snowpack in western North America. *Bulletin of the American Meteorological Society* **86**(1): 39–49.

Mote PW, Salathé EP. 2010. Future climate in the Pacific Northwest. *Climatic Change* **102**: 29–50.

Muzik I. 2002. A first-order analysis of the climate change effect on flood frequencies in a subalpine watershed by means of a hydrological rainfall–runoff model. *Journal of Hydrology* **267**(1): 65–73.

Neiman PJ, Schick LJ, Ralph FM, Hughes M, Wick GA. 2011. Flooding in western Washington: the connection to atmospheric rivers*. *Journal of Hydrometeorology* **12**(6): 1337–1358.

Nolin AW, Daly C. 2006. Mapping "at risk" snow in the Pacific Northwest. *Journal of Hydrometeorology* **7**(5): 1164–1171.

O'Connor JE, Costa JE. 2004a. Spatial distribution of the largest rainfall-runoff floods from basins between 2.6 and 26,000 km^2 in the United States and Puerto Rico. *Water Resources Research* **40**: W01107. DOI:10.1029/2003WR002247.

O'Connor JE, Costa JE. 2004b. The World's largest floods, past and present-their causes and magnitudes: U.S. Geological Survey Circular 1254, 13.

O'Connor JE, Grant GE, Costa JE. 2002. The geology and geography of floods. In *Ancient Floods, Modern Hazards: Principles and Application of Paleoflood Hydrology*, House PK, Webb RH, Baker VR, Levish DR (eds). American Geophysical Union Water Science and Application Series, No. 5. American Geophysical Union: Washington, DC; 359–385.

Prudhomme C, Jakob D, Svensson C. 2003. Uncertainty and climate change impact on the flood regime of small UK catchments. *Journal of Hydrology* **277**(1): 1–23.

R Core Team. 2014. R: A language and environment for statistical computing. R Foundation for Statistical Computing, Vienna, Austria. URL http://www.R-project.org/ (Last accessed on 22 May 2015).

Ragonda SK, Rajagopalan B, Clark M, Pitlick J. 2005. Seasonal cycle shifts in hydroclimatology over the western United States. *Journal of Climate* **18**(2): 372–384.

Ralph FM, Neiman PJ, Wick GA, Gutman SI, Dettinger MD, Cayan DR, White AB. 2006. Flooding on California's Russian River: Role of atmospheric rivers. *Geophysical Research Letters* **33**(13). DOI:10.1029/2006GL026689.

Reynard NS, Prudhomme C, Crooks SM. 2001. The flood characteristics of large UK rivers: potential effects of changing climate and land use. *Climatic Change* **48**(2-3): 343–359.

Rieman BE, Smith CL, Naiman RJ, Ruggerone GT, Wood CC, Huntly C, Merrill EN, Alldredge JR, Bisson PA, Congleton J, Fausch KD, Levings C, Pearcy W, Scarnecchia D, Smouse P. 2015. A comprehensive approach for habitat restoration in the Columbia basin. *Fisheries* **40**(3): 124–135. DOI:10.1080/03632415.2015.1007205.

Safeeq M, Grant GE, Lewis SL, Tague C. 2013. Coupling snowpack and groundwater dynamics to interpret historical streamflow trends in the western United States. *Hydrological Processes* **27**(5): 655–668.

Safeeq M, Grant GE, Lewis SL, Kramer MG, Staab B. 2014. A hydrogeologic framework for characterizing summer streamflow sensitivity to climate warming in the Pacific Northwest, USA. *Hydrology and Earth System Sciences* **18**: 1–18.

Salazar S, Francés F, Komma J, Blume T, Francke T, Bronstert A, Blöschl G. 2012. A comparative analysis of the effectiveness of flood management measures based on the concept of" retaining water in the landscape" in different European hydro-climatic regions. *Natural Hazards and Earth System Science* **12**(11): 3287–3306.

Seibert J, McGlynn BL. 2007. A new triangular multiple flow direction algorithm for computing upslope areas from gridded digital elevation models. *Water Resources Research* **43**(4). DOI:10.1029/2006WR005128.

Smith JA, Baeck ML, Steiner M, Miller AJ. 1996. Catastrophic rainfall from an upslope thunderstorm in the central Appalachians: the Rapidan storm of June 27, 1995. *Water Resources Research* **32**(10): 3099–3113.

Spracklen DV, Mickley LJ, Logan JA, Hudman RC, Yevich R, Flannigan MD, Westerling AL. 2009. Impacts of climate change from 2000 to 2050 on wildfire activity and carbonaceous aerosol concentrations in the western United States. *Journal of Geophysical Research* **114**(D20301): 1–17.

Stewart IT, Cayan DR, Dettinger MD. 2005. Changes toward earlier streamflow timing across western North America. *Journal of climate* **18**(8): 1136–1155.

Sturdevant-Rees P, Smith JA, Morrison J, Baeck ML. 2001. Tropical storms and the flood hydrology of the central Appalachians. *Water Resources Research* **37**(8): 2143–2168.

Sumioka SS, Kresch DL, Kasnick KD. 1998. Magnitude and frequency of floods in Washington: U.S. Geological Survey Open-File Report 97-4277.

Tague C, Grant GE. 2009. Groundwater dynamics mediate low-flow response to global warming in snow-dominated alpine regions. *Water Resources Research* **45**(7). DOI:10.1029/2008WR007179.

Tohver IM, Hamlet AF, Lee SY. 2014. Impacts of 21st-century climate change on hydrologic extremes in the Pacific Northwest Region of North America. *JAWRA* **50**(6): 1461–1476.

U.S. Water Resources Council. 1981. Guidelines for determining flood flow frequency: U.S. Water Resources Council Bulletin 17B, 28, 14 appendixes.

Westerling AL, Hidalgo HG, Cayan DR, Swetnam TW. 2006. Warming and earlier spring increase western US forest wildfire activity. *Science* **313**(5789): 940–943.

Wiley JB, Atkins Jr. JT, Tasker GD. 2000. Estimating magnitude and frequency of peak discharges for rural, unregulated streams in West Virginia: U.S. Geological Survey Water-Resources Investigations Report 00–4080, 93.

Wilby RL, Beven KJ, Reynard NS. 2008. Climate change and fluvial flood risk in the UK: more of the same? *Hydrological Processes* **22**(14): 2511–2523.

SUPPORTING INFORMATION

Additional supporting information may be found in the online version of this article at the publisher's web site.